F. Cherchi, M. Porru and A. Serpi, "Control System Design of a Stacked-Interleaved Buck Converter for Electrolysers," 2025 IEEE Vehicle Power and Propulsion Conference (VPPC), Hangzhou, China, 2025, pp. 1-5.



**The publisher's version is available at:**

http://dx.doi.org/10.1109/VPPC66000.2025.11393022

# Control System Design of a Stacked-Interleaved Buck Converter for Electrolysers

Francesco Cherchi, Mario Porru, Alessandro Serpi
*Department of Electrical and Electronic Engineering*
*University of Cagliari*
Cagliari, Italy

***Abstract*—The design of a multi-loop control system for a Stacked Interleaved Buck Converter (SIBC) is presented in this paper. Starting from the SIBC model, which reveals a significant coupling among the several voltage and current variables, a nested control loop structure has been defined to regulate the SIBC output voltage, branch currents and voltages simultaneously. The proposed design approach is based on the dynamic decoupling between the different control loops, which has been achieved by an appropriate management of SIBC model, as well as by introducing suitable auxiliary variables. The effectiveness of the proposed control system has been verified in simulations, which regards the tracking of a given reference output voltage profile in case of different and variable output currents.**

***Keywords—Control system design, Electrolysers, Stacked-Interleaved Buck Converter***

## I. Introduction

The decline in crude oil supplies, the political instability in regions with large oil reserves, and strict regulations on emissions in several countries have highlighted the need for alternative fuels [1] and innovative energy carriers, such as hydrogen produced from Renewable Energy Sources (RESs) [2]. However, the natural variability that characterizes RES production is well known, and this does not comply with hydrogen production by electrolysis of water, which requires stable and consistent electrical power supply. Therefore, the use of power electronic conversion systems are needed to interface RES with electrolysers in order to eliminate voltage/current/power fluctuations, thus successfully controlling their production.

Electrolysers operate at very low DC voltages, and require smooth and reliable power supplies [3]. Consequently, a direct power supply from the electrical network is not possible because of its AC nature, and due to rated grid voltages much higher than those required by electrolysers. A direct supply from photovoltaic cells or modules is problematic as well, because of their inherent power oscillations due to variable weather conditions. In this regard, it has been demonstrated that power supply oscillations significantly impair efficiency and useful life of electrolysers, whether they occur at high or low frequencies [4], [5]. Stacking several photovoltaic and electrolytic cells could be a solution to cope with voltage mismatches, but the number of cells that can be stacked is limited, not allowing reaching adequate power ratings [5], [6].

Power electronic converters are thus needed to interface electrolysers with different power supplies. However, conventional configurations enable a fair voltage adaptation with increasingly higher efficiencies, but they are characterized by high output current ripple. For this reason, novel configurations have been designed to achieve constant output current and voltage. Among these, the Stacked Interleaved Buck Converter (SIBC) is able to suppress the output current ripple by a suitable circuit topology and an appropriate switching pattern [3], [5], [6], [7], [8], [9], [10], so it is particularly suitable for electrolyser supply. Despite the operating principle of the SIBC is quite straightforward, the increased number of its devices compared to conventional configurations make its control system difficult to design. As a result, simplified control approaches can be employed, but SIBC dynamic performance cannot be optimized properly.

In this context, an advanced control system for SIBCs is proposed in this paper. Differently from conventional approaches, which generally regulate the output voltage directly through the duty cycle, the proposed control system consists of several nested control loops that regulate output voltage, branch currents and voltages in cascade to achieve the desired dynamic and steady-state performance. This goal has been achieved by an accurate management of the several cross-coupling effects that occur among different current and/or voltage variables. In particular, the dynamic decoupling between adjacent control loops has been imposed, as well as introducing auxiliary variables to improve the dynamic performance of the inner control loops. The effectiveness of the proposed SIBC control system has been verified by a simulation study, which regards the supply of an electrolyser by tracking a given reference output voltage at different operating conditions.

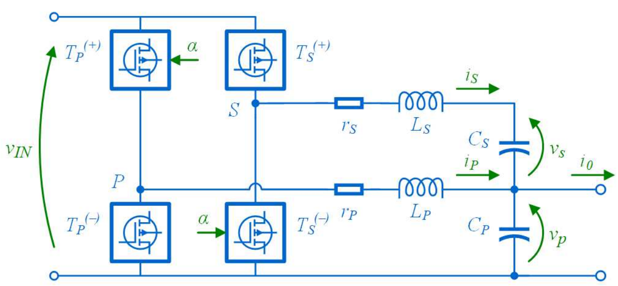


Fig. 1. Schematic representation of an SIBC.

## II. SIBC Overview

### *A. Operating principle*

Considering the overview of the SIBC shown in Fig. 1, it consists mainly of two branches, namely the P and the S branch. The P branch can be modelled by an inductor ($L_P$) and its series resistance ($r_P$), and it is alternatively supplied by the input voltage ($v_{IN}$) or short-circuited depending on the state of the switches $T_P^{(+)}$-$T_P^{(-)}$. The task of the P branch is carrying the DC current from the input to the output stage of the SIBC, storing energy into $L_P$ during the P-ON state (Fig. 2a), by delivering it to the output capacitor ($C_P$) and the load during the S-ON state (Fig. 2b). Differently, the S branch consists of an inductor ($L_S$), its series resistance ($r_S$), and a capacitor ($C_S$). The latter is alternatively charged and discharged during the S-ON and P-ON states, respectively. Consequently, its voltage can be kept constant at steady-state operation, meaning that only an AC current component can flow through the S branch at this operating condition.

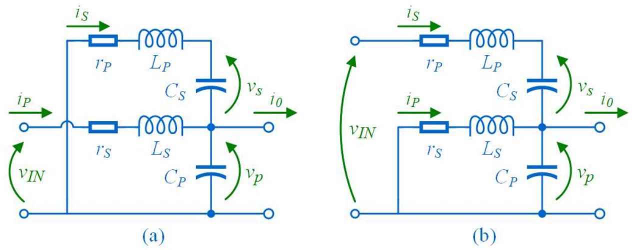


Fig. 2. SIBC operating states: a) P-ON, and b) S-ON.

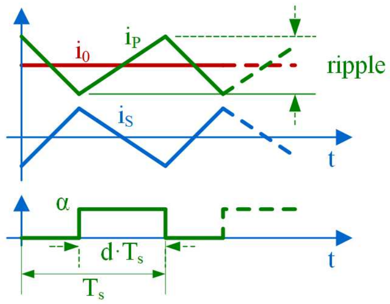


Fig. 3. SIBC command signal ($\alpha$) and current ripple cancellation effect.

Regarding the switches, the SIBC requires driving $T_P^{(+)}$-$T_S^{(-)}$ with the same command signal ($\alpha$), and $T_P^{(-)}$-$T_S^{(+)}$ with its complimentary signal. Assuming twin inductors ($r_P = r_S = r$, $L_P = L_S = L$), this results in the AC current components flowing into P and S branches being opposite to each other, thus no load current ripple theoretically occurs, as shown in Fig. 3; this is the main advantage of employing the SIBC configuration. In particular, the current ripple cancellation effect enables smaller inductors than traditional DC-DC converters as there is no need for filtering high-frequency current components, with a reduction in weight, size and costs, as well as lower losses and, therefore, better efficiency [13].

### *B. Mathematical modelling*

Considering the SIBC operating states shown in Fig. 2, the command signal $\alpha$ shown in Fig. 3, and assuming twin inductors, the mathematical model of the SIBC can be expressed as

$$\begin{aligned} \alpha v_{IN} &= r i_P + L\frac{di_P}{dt} + v_P\,, \quad C_P\frac{dv_P}{dt} = i_P + i_S - i_0 \\ (1-\alpha)v_{IN} &= r i_S + L\frac{di_S}{dt} + v_S + v_P\,, \quad C_S\frac{dv_S}{dt} = i_S \end{aligned} \tag{1}$$

where $i$ and $v$ denote currents and voltages of P branch, S branch, and load. It can be seen that the output voltage ($v_0 = v_P$) depends on the load current and on the sum between P and S currents. Consequently, summing the P and S voltage equations to each other yields

$$v_{IN} = r i_{PS} + L\frac{d i_{PS}}{dt} + v_S + 2v_P \tag{2}$$

in which $i_{PS} = i_P + i_S$. The latter equation does not depend on $\alpha$, revealing that $i_{PS}$ can be controlled by $v_S$ because $v_{IN}$ and $v_P$ are generally constrained by input and output voltage requirements.

The average mathematical model of the SIBC can be achieved by replacing the command signal $\alpha$ in (1) with its duty cycle ($d$), leading to:

$$\begin{aligned} d\,\overline{v}_{IN} &= r\overline{i}_P + L\frac{d\,\overline{i}_P}{dt} + \overline{v}_P\,, \quad C_P\frac{d\,\overline{v}_P}{dt} = \overline{i}_{PS} - i_0 \\ (1-d)\overline{v}_{IN} &= r\overline{i}_S + L\frac{d\,\overline{i}_S}{dt} + \overline{v}_S + \overline{v}_P\,, \quad C_S\frac{d\,\overline{v}_S}{dt} = \overline{i}_S \end{aligned} \tag{3}$$

$$\overline{v}_{IN} = r\overline{i}_{PS} + L\frac{d\,\overline{i}_{PS}}{dt} + \overline{v}_S + 2\overline{v}_P \tag{4}$$

where $^{-}$ denotes average values. Therefore, at steady-state operation ($d = D$), neglecting resistive voltage drops yields

$$\begin{aligned} \overline{v}_P &= D\overline{v}_{IN}\,, \quad \overline{i}_P = \overline{i}_0 \\ \overline{v}_S &= (1-2D)\overline{v}_{IN}\,, \quad \overline{i}_S = 0\,. \end{aligned} \tag{5}$$

In conclusion, (5) states that the output voltage is always smaller than the input voltage, confirming the buck effect. Also $v_S$ has a magnitude always smaller than $v_{IN}$, but it can be either positive or negative depending on D < 0.5 or not.

## III. Control System Design

The overview of the proposed SIBC control system is shown in Fig. 4, which consists of a number of nested control loops, each of which is based on a Proportional-Integral (PI) controller. Assuming that the electrolyser model is unknown, the outer control loop regulates the output voltage to the desired reference value; given (3), this task can be accomplished through $i_{PS}$, which, in turn, can be controlled by $v_S$ in accordance with (4). Finally, $v_S$ can be controlled by $d$ in accordance with (3), as detailed in the following subsections.

### *A. Output voltage control loop*

This control loop has been designed based on (3); particularly, the output voltage can be controlled through $i_{PS}$, whose reference profile can be synthesized by a PI controller. In this regard, even if a feedforward compensation of $i_0$ is concerned, a PI controller is needed in order to account for simplified modelling, uncertainties, and leakage currents. Therefore, the system and PI controller transfer functions are:

$$G_P = \frac{\overline{v}_P}{\overline{i}_{PS}} = \frac{1}{C_P s}\,, \quad R_P = \frac{k_P^{(P)}}{s}\left(s + \frac{k_I^{(P)}}{k_P^{(P)}}\right) \tag{6}$$

where $s$ is the Laplace's variable, while $k_P^{(P)}$ and $k_I^{(P)}$ are the proportional and integral gains, respectively. The closed loop transfer function is thus

$$W_P = \frac{\overline{v}_P}{\overline{v}_P^*} = \frac{k_P^{(P)}}{C_P}\cdot\frac{s + \frac{k_I^{(P)}}{k_P^{(P)}}}{s^2 + \frac{k_P^{(P)}}{C_P}s + \frac{k_I^{(P)}}{C_P}}\ . \tag{7}$$

Consequently, assuming $k_P^{(P)}$ large enough, $W_P$ has one zero ($z$) and two real poles ($p_1$ and $p_2 > p_1$), whose values depend on the PI controller gains; as $k_P^{(P)}$ increases, $p_2$ converges to $z$, whereas $p_1$ decreases. Consequently, the dynamic performance of this loop depends on $p_1$ mostly, which can be set at the desired value. Furthermore, the residual of $p_1$ can be set sufficiently large (i.e. $\xi$ times that of $p_2$, with $\xi >> 1$) in order to achieve a proper zero-pole cancellation effect. As a result, given the desired bandwidth $f_c^{(P)}$, the following design

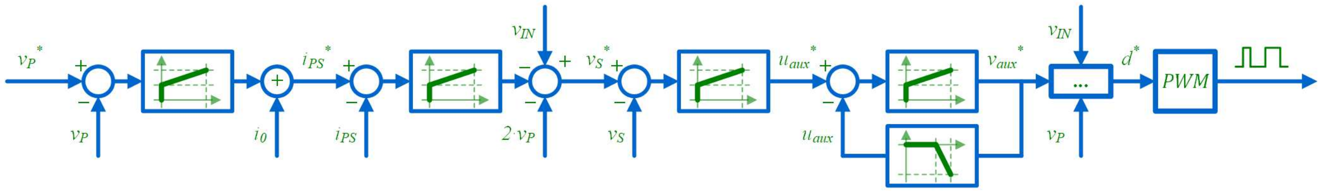


Fig. 4. The proposed equivalent block control scheme of the SIBC.

equations hold:

$$k_P^{(P)} = 2\pi f_c^{(P)} C_p \frac{1+\xi}{\xi}, \quad k_I^{(P)} = k_P^{(P)} \cdot 2\pi f_c^{(P)} \frac{1}{1+\xi} \ . \tag{8}$$

### B. Intermediate current control loop

The $i_{PS}$ control loop is designed in accordance with (2). In particular, assuming that $v_P$ varies sufficiently slower than $i_{PS}$, it can be assumed almost constant in (2) for $i_{PS}$ control system design purposes, leading to the following transfer function:

$$G_{PS} = \frac{\bar{i}_{PS}}{\bar{v}_{eq}} = \frac{1}{r+Ls}, \quad \bar{v}_{eq} = v_{IN} - \bar{v}_S - 2\bar{v}_P \tag{9}$$

Therefore, $i_{PS}$ can be controlled by $v_{eq}$ through a PI controller, whose gains can be set in order to achieve a zero-pole cancellation and the desired bandwidth ($f_c^{(PS)}$) as

$$k_P^{(PS)} = 2\pi f_c^{(PS)} L, \quad k_I^{(PS)} = k_P^{(PS)} \cdot \frac{r}{L} \ . \tag{10}$$

### C. Inner voltage control loop

Considering that $i_{PS}$ is controlled by $v_{eq}$, and given (9), the only variable available to drive $v_{eq}$ to its reference value is $v_s$ because $v_{IN}$ is constant, and $v_P$ is constrained by its outer control loop. Consequently, (3) leads to:

$$(1-d)v_{IN} = rC_S \frac{d\bar{v}_S}{dt} + LC_S \frac{d^2\bar{v}_S}{dt^2} + \bar{v}_S + \bar{v}_P \tag{11}$$

The transfer function between $v_S$ and an auxiliary input volage can be thus expressed as

$$G_S = \frac{\bar{v}_S}{\bar{v}_{aux}} = \frac{1}{LC_S} \cdot \frac{1}{s^2 + \frac{r}{L}s + \frac{1}{LC_S}}, \quad \bar{v}_{aux} = (1-d)v_{IN} - \bar{v}_P \tag{12}$$

Since $G_S$ has two poles and no zero, $v_{aux}$ is not a suitable choice to control $v_S$ directly. Consequently, the additional variable $u_{aux}$ is introduced as

$$\bar{u}_{aux} = \frac{1}{1+\tau s}\bar{v}_{aux} \quad \rightarrow \quad \tilde{G}_S = \frac{\bar{v}_S}{\bar{u}_{aux}} = \frac{1}{LC_S} \cdot \frac{1+\tau s}{s^2 + \frac{r}{L}s + \frac{1}{LC_S}} \tag{13}$$

As a result, by regulating $v_S$ by $u_{aux}$ through a PI controller, the closed-loop transfer function becomes

$$W_P = \frac{\bar{v}_S}{\bar{v}_S^*} = \frac{k_P^{(S)}}{LC_S} \frac{\left(s + \frac{k_I^{(S)}}{k_P^{(S)}}\right)(1+\tau s)}{s\left(s^2 + \frac{r}{L}s + \frac{1}{LC_S}\right) + \frac{k_P^{(S)}}{LC_S}\left(s + \frac{k_I^{(S)}}{k_P^{(S)}}\right)(1+\tau s)} \tag{14}$$

Given (13) and (14), different scenarios may occur depending on the values of the poles of $\tilde{G}_S$, which can be denoted by $p_3$ and $p_4 > p_3$ in the following; in case they are real, $\tau$ and $k_I^{(S)}$ can be chosen suitably to achieve a double zero-pole cancellation, leading to

$$W_P\Big|_{p_3,p_4\in\Re} = \frac{k_P^{(S)}}{LC_S} \frac{1}{s + \frac{k_P^{(S)}}{LC_S}}, \quad \tau = -\frac{1}{p_3}, \quad k_I^{(S)} = -k_P^{(S)} p_4 \tag{15}$$

Therefore, $k_p^{(S)}$ can be chosen to achieve the desired bandwidth ($f_c^{(S)}$) as

$$k_P^{(S)} = 2\pi f_c^{(S)} LC_S \tag{16}$$

Otherwise, i.e. $p_3$ and $p_4$ are complex, $\tau$, $k_I^{(S)}$ and $k_p^{(S)}$ should be chosen synergistically based on (14) to achieve the desired dynamic performance and two fair zero-pole cancellation effects in the closed-loop transfer function.

Once the reference $u_{aux}$ profile has been achieved, it can be tracked by $v_{aux}$ and, thus, by $d$, in accordance with the following relationships:

$$G_u = \frac{\bar{u}_{aux}}{\bar{v}_{aux}} = \frac{1}{1+\tau s}, \quad R_u = \frac{k_P^{(u)}}{s}\left(s + \frac{k_I^{(u)}}{k_P^{(u)}}\right) \tag{17}$$

In particular, by imposing the desired bandwidth ($f_c^{(u)}$) and the zero-pole cancellation, the PI controller gains can be computed as

$$k_P^{(u)} = 2\pi f_c^{(u)} \tau, \quad k_I^{(u)} = k_P^{(P)} \cdot \frac{1}{\tau} \ . \tag{18}$$

In conclusion, it is worth noting that an appropriate dynamic decoupling should be imposed so that

$$f_c^{(P)} < f_c^{(PS)} < f_c^{(S)} < f_c^{(u)} < f_s \tag{19}$$

where $f_s$ denotes the SIBC switching frequency.

## IV. Simulations

### A. Setup

The proposed SIBC control system has been verified through simulations in MATLAB-Simulink; the simulation setup is shown in Fig. 5, while system and control parameters are resumed in TABLE I. and TABLE II. , respectively. In particular, the bandwidths have been designed in accordance with both (19) and the procedure described in the previous section, while the electrolyser is modelled by means of a current source.

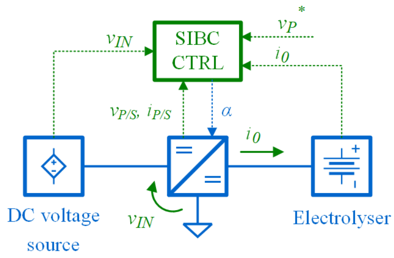


Fig. 5. Simulation setup.

TABLE I. SIBC PARAMETERS

| Parameter | Value | Unit |
|---|---|---|
| $v_{IN}$ | 24 | V |
| $v_{p,n}$ | 8 | V |
| $i_{0,n}$ | 25 | A |
| $r_P$, $r_S$ | 60 | mΩ |
| $L_P$, $L_S$ | 400 | µH |
| $C_P$ | 100 | µF |
| $C_S$ | 0.1 | F |

TABLE II. CTRL SYSTEM PARAMETERS

| Parameter | Value | Unit |
|---|---|---|
| $k_P^{(P)}$ | 10.5 | mA/V |
| $k_I^{(P)}$ | 98.7 | mA/V/s |
| $k_P^{(PS)}$ | 0.63 | V/A |
| $k_I^{(PS)}$ | 94.2 | V/A/s |
| $k_P^{(S)}$ | 5.0 | - |
| $k_I^{(S)}$ | 7000 | 1/s |
| $k_P^{(u)}$ | 125.6 | - |
| $k_I^{(u)}$ | 6283.2 | 1/s |

Simulations regard the start-up of the SIBC at first; particularly, the reference voltage signal varies from 0 to 8 V in 1 s, after which it becomes constant, while output current is kept constant at zero. At 2 s, the output current is linearly increased from 0 to 25 A in 4 s, then it is kept constant for a while. Starting from 10 s, a ramp-decreasing current is also concerned, i.e. $i_0$ is reduced from 25 A to 12.5 A in 2 s to test the effectiveness of the proposed control system at different operating conditions.

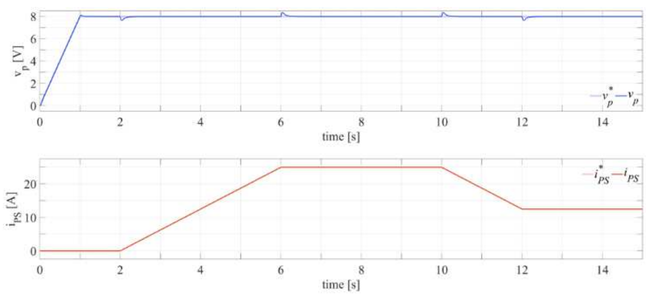


Fig. 6. The $v_P$ and $i_{PS}$ reference and actual evolutions.

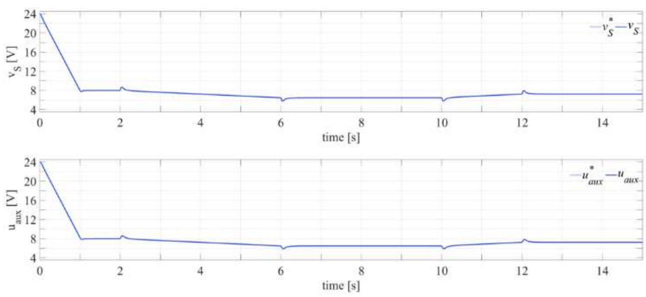


Fig. 7. The $v_S$ and $u_{aux}$ reference and actual evolutions.

## B. Results

Simulation results are shown from Fig. 6 to Fig. 10. Focusing on SIBC start-up at first, it can be seen that $v_P^*$ is very well tracked (Fig. 6), although a small overshoot occurs immediately after $v_p^*$ reaches its constant value. Even better tracking performance have been achieved for all the other reference profiles ($i_{PS}^*$, $v_s^*$, and $u_{aux}^*$, Fig. 6-Fig. 7), while the duty cycle $d$ (Fig. 8) increases from 0 to its corresponding steady-state value (~0.33). It is worth noting that $i_{PS}$ is very small during SIBC start-up as no load current occurs, so it cannot be detectable in Fig. 6. However, appropriate current control is revealed by Fig. 9, which shows that $i_P$ increases and $i_S$ decreases in a symmetrical fashion so that $v_P$ and $v_S$ can be driven to their corresponding reference value. Once $v_P^*$ has been achieved, both these currents are restored at zero apart from the inherent ripple due to the SIBC switching.

When $i_0$ increases, a small $v_P$ drop occurs at first (Fig. 6), after which $v_P$ is restored to its reference value. Small but sudden variations transiently occur on $v_s^*$ and $u_{aux}^*$ (Fig. 7), as well as some dips and/or spikes on $d$, $i_P$, and $i_S$ (Fig. 8-Fig. 9); these are caused by the $v_P$ drop, which forces all the other variables to compensate for it. Similar considerations apply when $i_0$ reaches its maximum value (at 6 s), as well as for the subsequent decreasing ramp (from 10 to 12 s), thus revealing the effectiveness of the proposed control approach.

In conclusion, the steady-state current evolutions are shown in Fig. 10, which refer to six switching time intervals around 15 s. This figure reveals the achievement of the current ripple cancellation effect as $i_P$ variations are opposite to $i_S$, thus leading to a negligible current ripple on $i_{PS}$, as expected.

## V. CONCLUSIONS

A cascade control system architecture for a Stacked Interleaved Buck Converter (SIBC) to supply an electrolyser is presented in this paper. It consists of a number of nested control loops that aim at achieving adequate dynamic decoupling among the main SIBC variables, as well as enhanced dynamic performance in regulating the output voltage of the converter. The effectiveness of the proposed approach has been verified by a simulation study, which

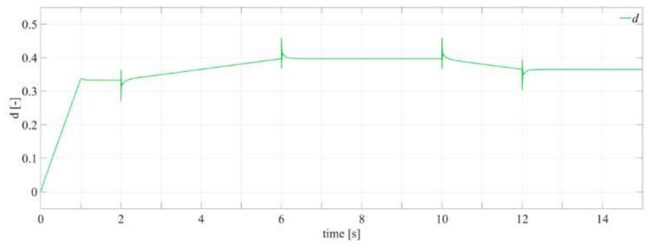


Fig. 8. The evolution of d.

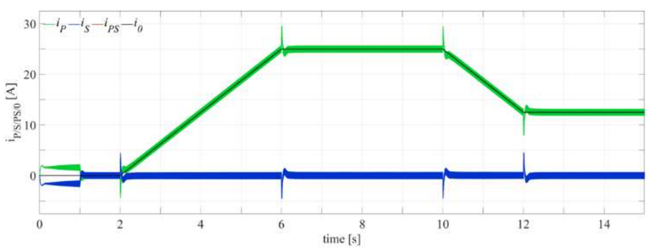


Fig. 9. The $i_P$, $i_S$, $i_{PS}$, and $i_0$ evolutions.

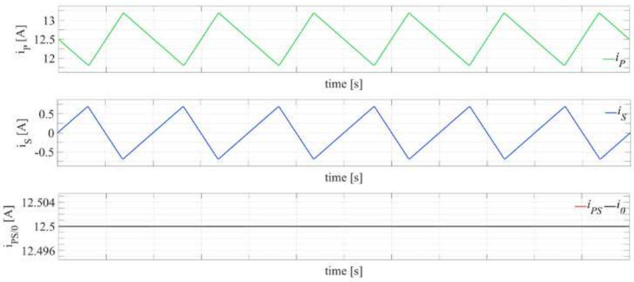


Fig. 10. The $i_P$, $i_S$, $i_{PS}$, and $i_0$ evolutions at steady-state operation.

reveals a good SIBC operation at different operating conditions. Several further improvements can be introduced, among which an enhanced design of the proposed control system by considering the electrolyser model. The latter also enables adding a further outer control loop to regulate the electrolyser current appropriately. These and other aspects will be investigated in future works, as well as experimental validation.

## Acknowledgment

This work is partially developed within the project PROMETH2eus ("Production of green $H_2$ from sea water by a novel electrolyser operating at high temperature and integrated with a power-to METhanol process", ID RSH2A_000039, CUP F37G22000080006), funded by MASE under the call PNRR M2C2 I3.5.

## References

[1] A. Campen, K. Mondal, and T. Wiltowski, "Separation of hydrogen from syngas using a regenerative system," *Int. J. Hydrog. Energy*, vol. 33, no. 1, pp. 332–339, Jan. 2008, doi: 10.1016/j.ijhydene.2007.07.016.

[2] A. Kovač, M. Paranos, and D. Marciuš, "Hydrogen in energy transition: A review," *Int. J. Hydrog. Energy*, vol. 46, no. 16, pp. 10016–10035, Mar. 2021, doi: 10.1016/j.ijhydene.2020.11.256.

[3] B. Yodwong, D. Guilbert, M. Phattanasak, W. Kaewmanee, M. Hinaje, and G. Vitale, "Proton Exchange Membrane Electrolyzer Modeling for Power Electronics Control: A Short Review," *J. Carbon Res.*, vol. 6, no. 2, Art. no. 2, Jun. 2020, doi: 10.3390/c6020029.

[4] F. da Costa Lopes and E. H. Watanabe, "Experimental and theoretical development of a PEM electrolyzer model applied to energy storage systems," in *2009 Brazilian Power Electronics Conference*, Sep. 2009, pp. 775–782. doi: 10.1109/COBEP.2009.5347619.

[5] D. Guilbert, S. M. Collura, and A. Scipioni, "DC/DC converter topologies for electrolyzers: State-of-the-art and remaining key issues," *Int. J. Hydrog. Energy*, vol. 42, no. 38, pp. 23966–23985, Sep. 2017, doi: 10.1016/j.ijhydene.2017.07.174.

[6] B. Yodwong, D. Guilbert, W. Kaewmanee, and M. Phattanasak, "Energy Efficiency Based Control Strategy of a Three-Level Interleaved DC-DC Buck Converter Supplying a Proton Exchange Membrane Electrolyzer," *Electronics*, vol. 8, no. 9, Art. no. 9, Sep. 2019, doi: 10.3390/electronics8090933.

[7] V. Guida, D. Guilbert, G. Vitale, and B. Douine, "Design and Realization of a Stacked Interleaved DC–DC Step-Down Converter for PEM Water Electrolysis with Improved Current Control," *Fuel Cells*, vol. 20, no. 3, pp. 307–315, 2020, doi: 10.1002/fuce.201900153.

[8] D. Guilbert, D. Sorbera, and G. Vitale, "A stacked interleaved DC-DC buck converter for proton exchange membrane electrolyzer applications: Design and experimental validation," *Int. J. Hydrog. Energy*, vol. 45, no. 1, pp. 64–79, Jan. 2020, doi: 10.1016/j.ijhydene.2019.10.238.

[9] R. R. Makineni, D. Sutanto, K. M. Muttaqi, Md. R. Islam, and A. P. Agalgaonkar, "Dual Loop Cascade Control of a Stacked Interleaved Buck Converter for Electrolyzer Application," in *2022 IEEE IAS Global Conference on Emerging Technologies (GlobConET)*, May 2022, pp. 1029–1035. doi: 10.1109/GlobConET53749.2022.9872460.

[10] H. Renaudineau, A. M. Llor, R. Cortés D., C. A. Rojas, C. Restrepo, and S. Kouro, "Photovoltaic Green Hydrogen Challenges and Opportunities: A Power Electronics Perspective," *IEEE Ind. Electron. Mag.*, vol. 16, no. 1, pp. 31–41, Mar. 2022, doi: 10.1109/MIE.2021.3120705.